

# The Porosity-Depth Pattern Defined by 40 Wells in Eugene Island South Addition, Block 330 Area, and its Relation to Pore Pressure, Fluid Leakage, and Seal Migration

---

## Andre Revil

Centre National de la Recherche Scientifique  
Centre European de Recherche et d'Education en Geosciences de l'Environnement  
Department of Geophysics  
University of Aix-Marseille III  
Aix-en-provence, France  
e-mail: revil@cerege.fr

## L. M. Cathles

Department of Earth and Atmospheric Sciences  
Cornell University, Ithaca, N.Y. 14853  
email: cathles@geology.cornell.edu

## Abstract

Porosity-depth profiles determined from density logs in numerous wells in the Eugene Island South Addition Block 330 area of the offshore Louisiana Gulf of Mexico show departures from the expected hydrostatic compaction trends at depths ranging from 900 m to 1950 m. At greater depths, porosities may remain constant, increase, or decrease. Although it changes over distances of a few kilometers, the porosity pattern is locally coherent. The cause of porosity departure from the expected compaction related trend (hydrostatic trend) is in all observed cases pore pressures in excess of hydrostatic pressures.

Porosity profiles are plotted and analyzed in detail in 40 area wells. Fluid pressure in these wells can be predicted from porosity because porosity is linearly related to effective stress. The depth at which porosity departs from the hydrostatic trend (the porosity-defined top of overpressure) coincides mostly with the 1.27 Ma transgressive *Helicosphaera sellii* shale that immediately overlies the gas-charged "JD" sand. However, in Block 314, the porosity-defined top of overpressure lies 500 m above the *H. sellii* surface, passing above two sand units and two transgressive shales.

In this paper we derive analytical expressions that were used to interpret porosity profiles and overpressure relationships. One well in Block 314 was analyzed in detail as an example. In this well a seal was developed in the *H. sellii* shale when the shale lay at ~550m depth. When this lithologically fixed seal was gradually buried to 1430m depth, fluid pressures in underlying strata reached 0.8 of lithostatic and the seal began to deform and leak. Continued leakage while the seal was buried to its present depth of 2020m produced an interval of constant porosity (migrating seal compartment) from 1040 to 2020m.

Although other interpretations are admittedly possible, we suggest that the migrating seal compartment formed when hydrocarbon fluids were introduced and capillary barriers developed. Applying the same methods, we identify areas in the Eugene Island South Addition Block 330 area where venting has diminished and areas where it has accelerated. The methods further developed and illustrated could facilitate exploration for higher porosity, more permeable sand reservoirs, address hazards associated with fluid overpressuring, and extract information on the timing and nature of hydrocarbon venting from a new information base: shale porosity profiles.



## Introduction

Shale porosity is of interest for many reasons:

1. Shale is the dominant lithology in many basins.
2. Expulsion of pore waters from shale could affect the pressure distribution and flow of pore waters and hydrocarbons throughout a basin.
3. In many cases (but not all), shale porosity depends only on effective stress (lithostatic stress minus pore pressure), and excess shale porosity provides a useful measure of pore fluid pressure.
4. Overpressured shales pose drilling hazards and promote slumping and fault movement.
5. Shale porosity profiles can reflect the history of overpressuring and the time of seal formation in an area.

This last of these reasons is our prime focus in this paper. We will, in the first section, present analytical disequilibrium compaction models for depth intervals with: (1) no overpressuring, (2) constant overpressuring, and (3) overpressuring that parallels lithostatic pressure (so porosity is constant). In later sections we will then apply these models to interpret the porosity profiles in over 40 wells in the Eugene Island Block 330 area.

To interpret shale porosity we need to know how shales compact when pore fluid is hydrostatically pressured. Hunt *et al.* (1998) have recently suggested that, except very near the surface, porosity decreases linearly with depth maintaining hydrostatic pressure conditions until porosities of ~10% are reached. At greater depths, the porosity remains constant. The boundary between linear (stage 1) compaction and no (stage 2) compaction typically occurs at the 90°C isotherm; although where sedimentation is rapid it lies at slightly greater depths (105°C isotherm). According to Hunt *et al.* (1998), the boundary occurs when the shale pores have been reduced to the thickness of about 3 monolayers of water. For shales with a high percentage of high surface area clays (illite + smectite + illite-smectite) the limit of normal compaction can be 15-20% or even greater. For shales with a low percentage of high surface area clays, the limit of compaction can be as low as 3%.

Hunt *et al.* (1998) point out that once shales reach Stage 2 compaction, shale porosity is independent of effective stress. If pore pressure is subsequently increased (by hydrocarbon maturation, for example), the porosity will not increase and the overpressures will not be reflected in shale porosity. Hunt *et al.* (1998) show several examples where the top of overpressure lies in the Stage 2 compaction zone and porosity remains unchanged, despite the large increase in pore pressure. The concept that there is a natural limit to shale compaction, with the additional criterion that subsequent increases in pore pressure do not de-compact the shales, provides a nice explanation of these otherwise difficult-to-understand observations, but means that porosity is not a reliable indicator of pore pressure. This contradicts a considerable literature that suggests that porosity data can be used to predict excess (above hydrostatic) pore pressures (*e.g.*, Magara, 1978; see also Fertl, 1976; Bray and Karig, 1985; Shi and Wang, 1988; Bangs *et al.*, 1990; Luo and Vasseur, 1992, 1993; Bour *et al.*, 1995; Hart *et al.*, 1995; Gordon and Flemings, 1998).

In this paper we examine the porosity-depth profiles and mud weight data in 89 wells (40 in detail) in the Eugene Island area to determine whether the intervals of approximately constant porosity are caused by compaction reaching its natural limit or by the development of fluid overpressure. By comparing the fluid pressures predicted from shale porosity to those computed from mud weight data, we find that the constant porosity intervals, where porosity exceeds ~20%, are in a state of disequilibrium compaction as Gordon and Flemings (1998) reported from their analysis of several wells in the same area. To analyze and interpret the pattern of compaction, we develop theoretical relations against which departures from hydrostatic compaction can be measured. We find that the pattern of subsurface shale porosity is spatially coherent on a local scale but varies smoothly and significantly over the study area. We define a surface where porosity begins to depart from the hydrostatic compaction trend. This surface parallels the *H. sellii* transgressive shale over much of the study area, but dramatically crosscuts lithology in Block 314. We develop a set of modular analytic expressions and use them to interpret the history of seal formation from this pattern. We suggest that the sediments become impermeable when hydrocarbon fluids entered the area and capillary seals formed (Cathles, 2001, this volume; Shosa and Cathles, 2001, this volume), but alternative interpretations are also possible.



## Excess Porosity in the Eugene Island Block 330 Area

Figure 1 shows the location of the study area as well as major faults, sands, and chrono-stratigraphic marker horizons within it. The Eugene Island study area is located about 160 km off the Louisiana coast. It contains an oblong (approximately 18 x 14 km), passive margin salt-withdrawal minibasin that is bounded by faults. The northern and eastern boundaries are regional down-to-the-south normal faults; counter-regional faults form the western and southern boundaries. Movement on these faults occurred as salt withdrew from beneath the minibasin. The minibasin is well described in Ph.D. dissertations and in the published literature (*cf.*, Holland *et al.* 1990; Alexander, 1995; Alexander and Flemings, 1995; Coelho, 1997; Alexander and Handschy, 1998).

The equations and methods used in our interpretation are developed in an Appendix to this paper. These equations assume that the conditions of disequilibrium compaction hold. This requires that porosity is linearly related to effective stress (as specified by equation (1), see Appendix), but also requires that: (1) fluid pressures have not increased for reasons unrelated to compaction, (2) solid material has not been dissolved and removed, (3) buoyant pressures are not transmitted horizontally or vertically, *etc.* Porosity is deduced from density logs using the relationship  $\rho = (1 - \phi)\rho_g + \phi\rho_f$ , where  $\rho$  is the sediment density,  $\rho_g$  is the sediment grain density, and  $\rho_f$  is the pore fluid density. Generally we take the grain density to equal 2650 kg/m<sup>3</sup> and set the pore fluid density equal to 1100.

The interpretation method is straightforward. The effective (neglecting very near surface compaction) uncompacted porosity,  $\phi_o$ , and the constant,  $\beta$ , that relates porosity changes to effective stress are determined by fitting an analytic expression for hydrostatic compaction (Equation 6, see Appendix) to the observed porosity-depth relation in the hydrostatically pressured portion of a well that has a density log. The hydrostatic porosity profile is extended to the non-hydrostatic parts of the well, and the non-hydrostatic porosity,  $\delta\phi$ , determined. The value for  $\delta\phi(z)$  is then substituted into Appendix equations (12) and (13) to obtain the excess fluid and lithostatic pressures as a function of depth. The total fluid and lithostatic pressures are provided by Appendix equation (10). Salinity was determined using methods described in Revil *et al.* (1998).

Porosity as a function of depth was analyzed in this fashion in 89 wells in the study area. Figure 2 shows that porosity is linearly related to effective stress. The linear relationship is tested in this figure mainly in the hydrostatic portions of 5 wells (filled circles), but is shown to also hold in about 11 cases where pore fluids are overpressured and mud weight measurements of fluid pressure allow effective stress to be calculated (open circles). The effective stress relationship of Equation (1) (see Appendix) holds equally well for hydrostatic and non-hydrostatic conditions (Fig. 2b). Figure 3 compares the fluid pressures predicted from excess porosity to fluid pressures inferred from 30 mud weight measurements. The fluid pressures predicted from excess porosity agree with the independent estimates from mud weight data. Our first important conclusion is that, in the Eugene Island area, excess porosity can be used to predict excess pore pressure at a useful level of accuracy.

Figure 4 plots porosity, excess fluid pressure, shale content (from gamma log analysis), pore fluid salinity, and sedimentation rate against depth for 40 of the 89 wells analyzed. This figure shows that, with only a few exceptions, porosity changes in the Eugene Island area are spatially coherent locally, but vary significantly over the study area. For example, the southwest third of Block 314 in Figure 4a has three wells where porosity departs from hydrostatic at about 1000 m depth and traps a constant porosity of 0.3 over a depth interval of ~1000 m, but the porosity profiles in a cluster of 6 wells at the boundary of Blocks 331 and 314 in Figure 4b depart from hydrostatic at 1500 m and trap porosities of ~0.25. The compaction parameters,  $\phi_o$  and  $\beta$ , vary in a smooth fashion across the study area (Table 1). Spatially clustered wells have very similar coefficients, although there are a few exceptions to this rule. Histograms of these parameters are plotted in Figure 5.



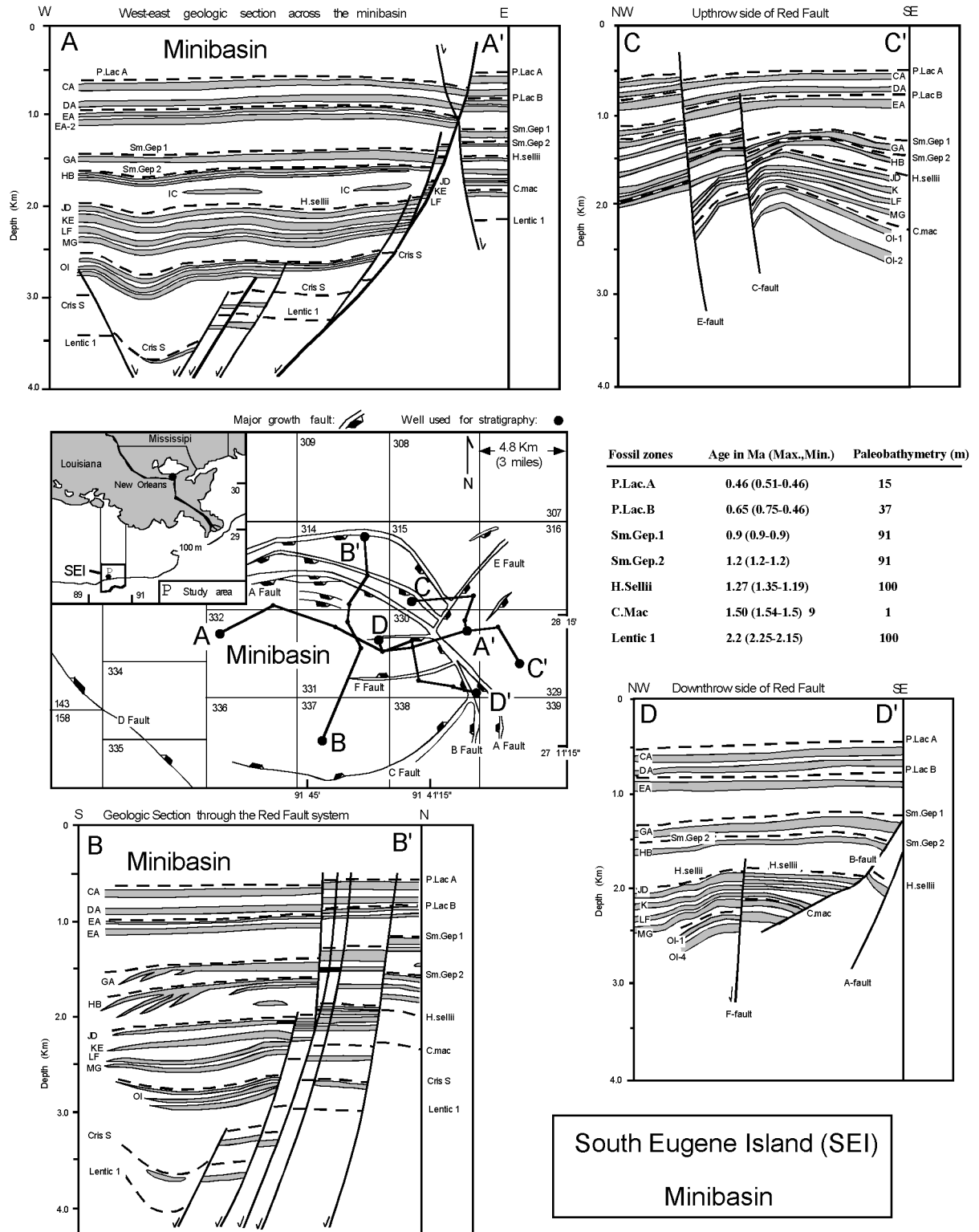


Figure 1. Location map and cross section showing the main faults and sand strata in the Eugene Block 330 minibasin. Sands are grey; time-stratigraphic marker horizons are black dashed lines. The cross sections are modified from interpretations of Alexander(1995), Alexander and Flemings (1995), and Coelho (1997).

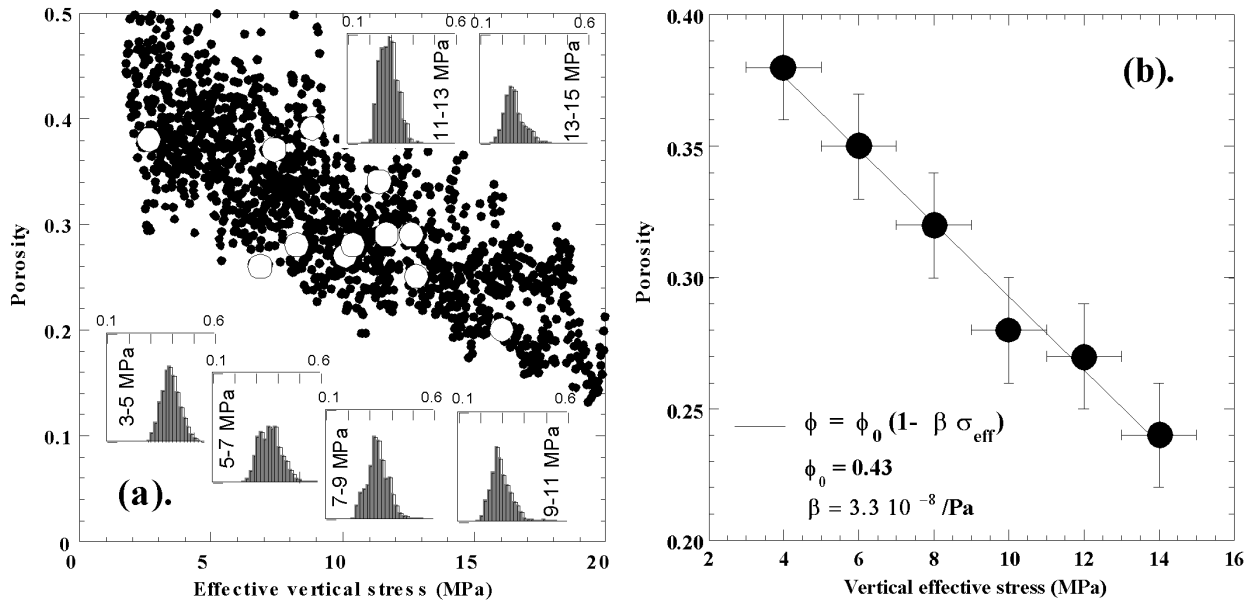


Figure 2. (a). Porosities calculated from downhole density logs in the hydrostatically pressured parts of five wells are plotted as filled circles against effective stress in the wells. Open circles plot porosities of overpressured formations where mud weight data have been used to calculate effective stress. From the gamma log response the sediments have a clay content ranging from 15% to 80% and an average of 60%. Only 5% of the hydrostatically pressured data are plotted to preserve clarity. The inset histograms include all the data. The histograms plot porosity (from 0.1 to 0.6) for 2 MPa intervals of effective stress starting at 3MPa. The scatter in porosity (spread in the histograms) arises from the fact that sediments with different proportions of sand and shale have different compressibility. (b). The average porosity from the histograms in (a) are plotted as a function of effective stress. Porosity is linearly related to effective stress. The average non-compacted porosity of sediments in the SEI 330 area is 0.43, and the average sediment compressibility is  $(3.3 \pm 0.3) \times 10^{-8} \text{ Pa}^{-1}$ .

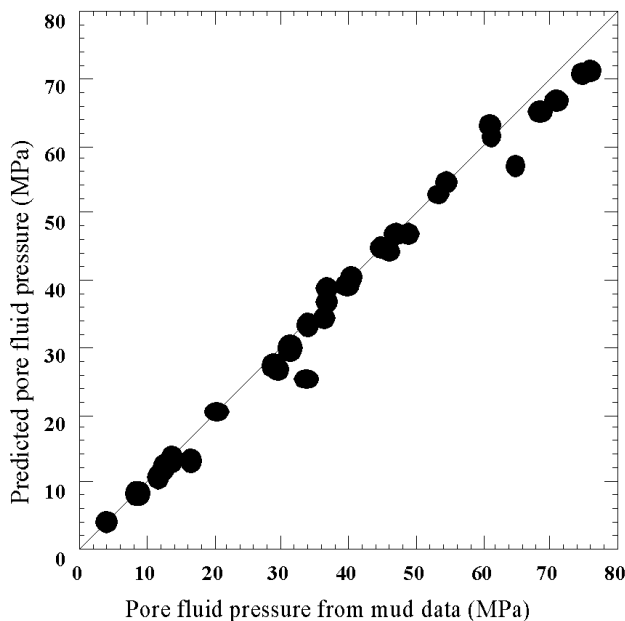
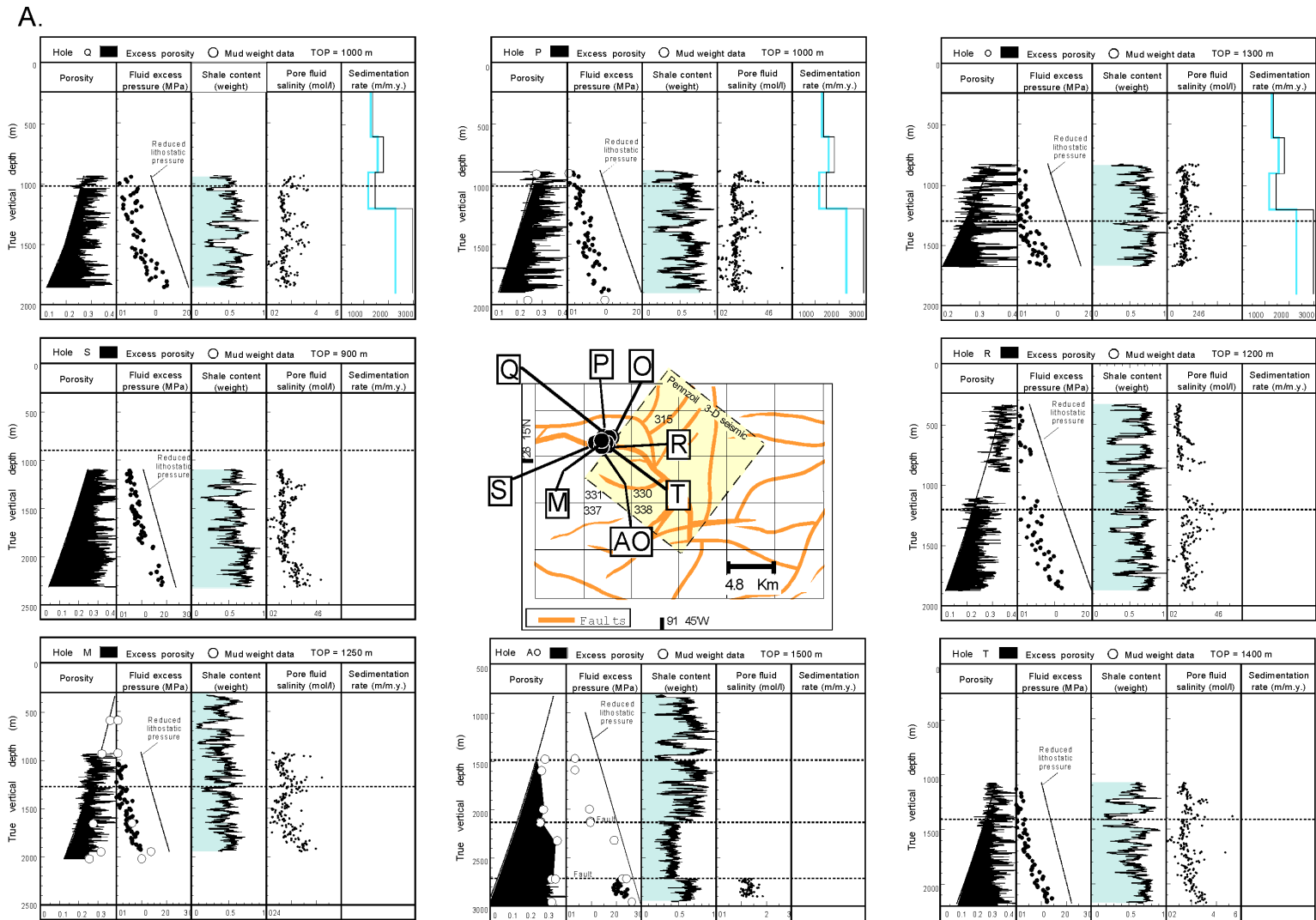


Figure 3. Pore fluid pressures predicted from excess porosity compared to fluid pressures inferred from mud weight data.





**Figure 4A.** Porosity, fluid overpressure, shale content in wt %, pore fluid salinity, and sedimentation rate for 40 wells in the SEI study area. Porosity is determined from density logs. Fluid overpressure is calculated from excess porosity. Reduced lithostatic pressure is obtained from numerical integration of sediment density. Reduced lithostatic pressure is defined as lithostatic pressure minus hydrostatic pressure. The sedimentation rate is determined from the stratigraphic ages given in Figure 1. The depth at which the porosity profile departs from hydrostatic is given for each profile in the heading of each plot. TOP is the depth at which porosity departs from hydrostatic porosity. Individual wells are located on the plan map insert. The shaded box indicated the outlines of the 3D seismic survey interpreted by Coelho (1997).



B.

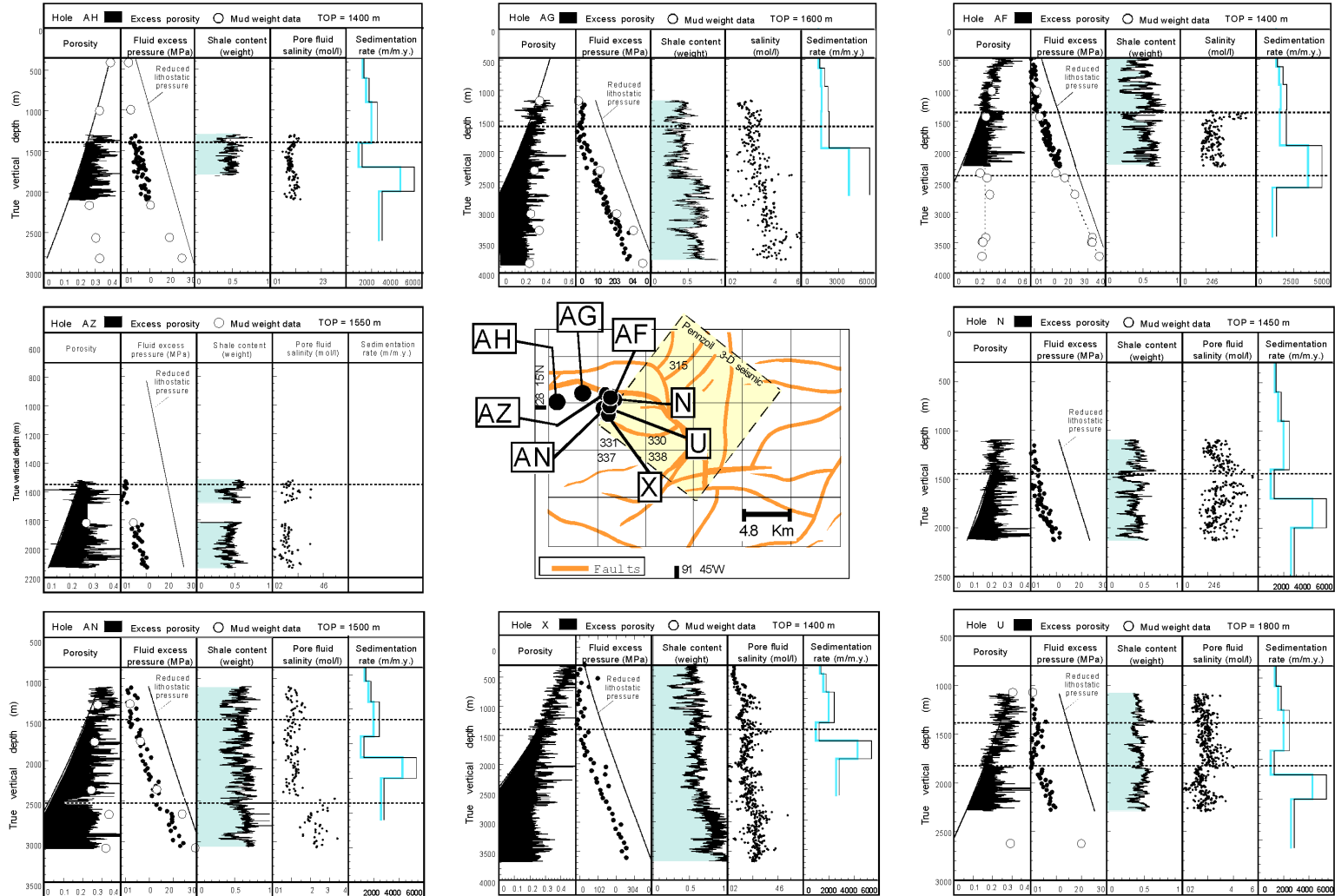


Figure 4B.



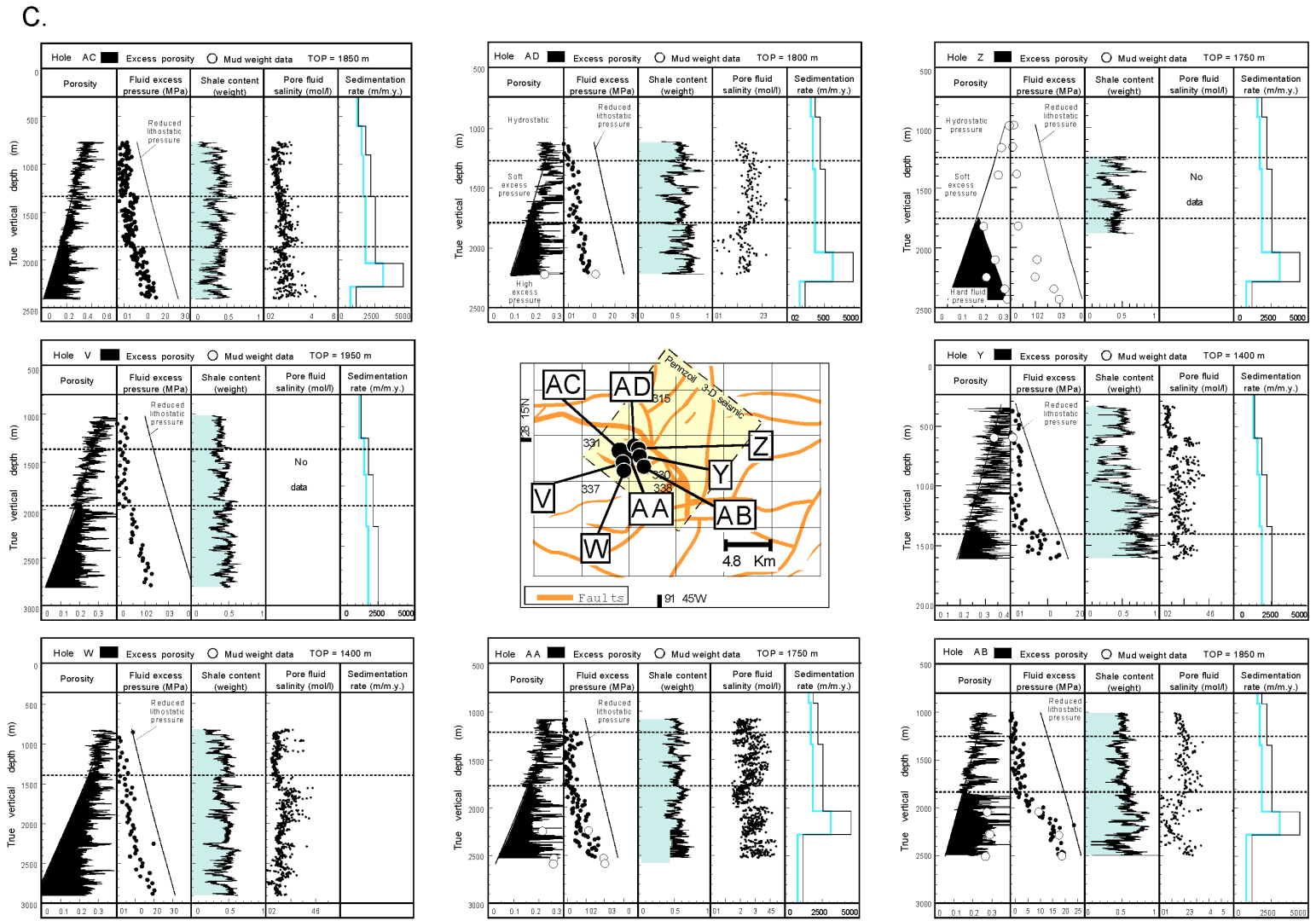


Figure 4C.



D.

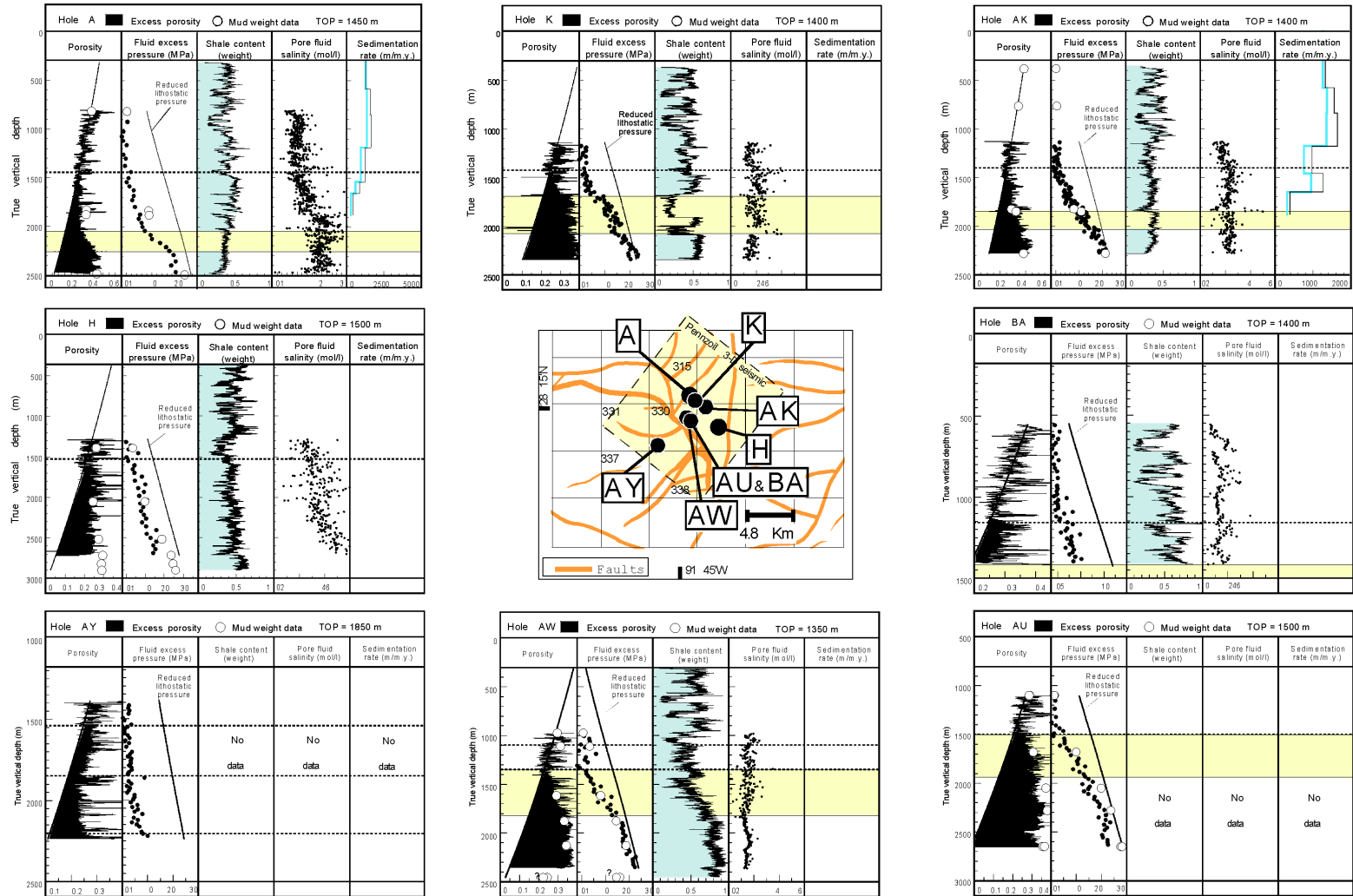


Figure 4D.



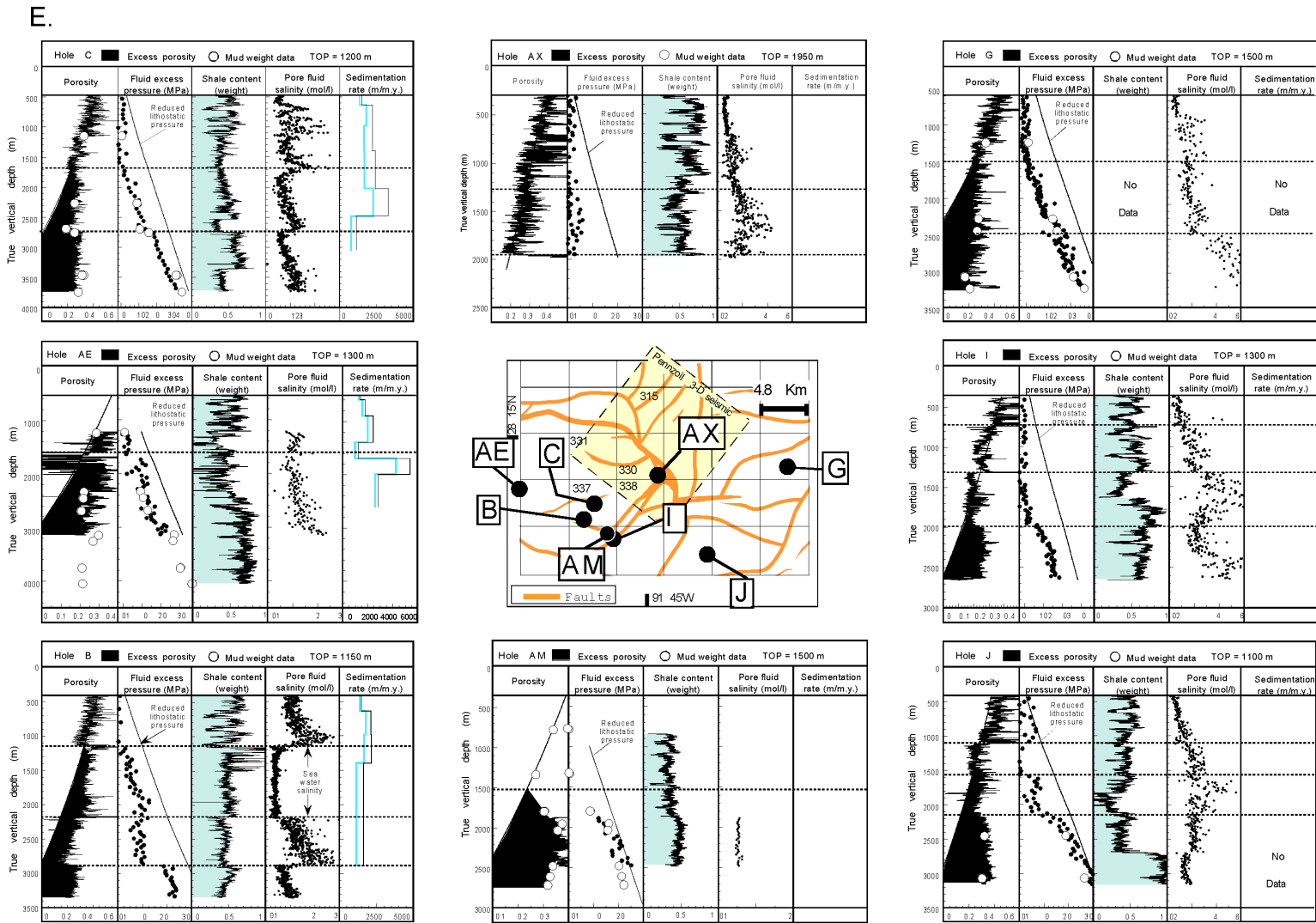


Figure 4E.



**Table 1. Summary of porosity-depth profiles in Figure 4. Well ID, letter code in Figure 4, and compaction parameters are listed.**

Well ID and Letter Code	$\phi_o$	$\beta \times 10^{-8}$	Trend	Porosity profile	Genetic type	Comments	
<b>Figure 4A (SW Block 314)</b>							
II-314EX-C13-409820	Q	0.38	3.0	c	0.3 (1000-1800)	M	
II-314EX-C11-411140	P	0.38	3.0	d	0.3 (1000) – 0.24 (1800)	fM	
II-314EX-C10-409990	O	0.43	3.0	c	0.3 (1300-1700)	M	
II-314EX-C7-409730	S	0.38	3.0	c	0.3 (900-2300)	M	
II-314EX-C2-409200	R	0.38	3.0	i	0.26 (1200) – 0.32 (2200)	sM	$\phi$ -corr sal chg
II-314EX6-407890	M	0.43	3.0	c	0.26 (1250-2000)	M	
I-314EX-C12-410830	AO	0.43	3.0	c,d	0.25 (1500-2100), 0.32 (2300-3000)	M-F	limited data
II-314EX-C9-409930	T	0.45	3.4	i	0.26 (1400) – 0.32 (2200)	sM	
<b>Figure 4B (Eastern boundary between Block 331, S Block 314)</b>							
I-313TX1-403770	AH	0.43	3.0	c	0.26 (1400-2000)	M	
I-313TX2-403590	AG	0.46	3.25	d	0.25 (1600) – 0.2 (4000)	fM	increase salinity
I-314EX-A1-402170	AF	0.42	3.4	c	0.25 (1400-2200)	M	
II-314HV-1-400200	AZ	0.48	3.4	c	0.26 (1550-2100)	M	
II-314EX-A21-405171	N	0.40	3.4	c	0.23 (1450-2200)	M	$\phi$ -corr sal chg
I-331SHB10-401910	AN	0.44	3.3	c	0.25 (1500-3000)	M	$\phi$ -unrelated sal chg
II-331SH-B1-401170	X	0.51	3.8	di	0.25 (1400) – 0.20 (2800) – 0.23 (3500)	fsM	
II-331SH-A14-401690	U	0.45	3.4	c	0.22 (1800-2300)	M	$\phi$ -corr sal chg
<b>Figure 4C (Boundary Blocks 330, 331)</b>							
II-331SH-A23-402230	AC	0.45	3.02	c	0.2 (1850-2400)	M	$\phi$ -corr sal chg
I-330PZ-A11-401080	AD	0.38	3.0	c	0.2 (1800-2200)	<b>M</b>	$\phi$ -corr sal chg
III-330PZ-A15-402470	Z	0.40	3.0	i	0.15 (1750) – 0.28 (2400)	F	limited data
II-331SH-A15-401920	V	0.45	3.0	c	0.2 (1950-2800)	M	
III-330PZ6-400980	Y	0.40	3.0	i	0.22 (1400) – 0.28 (2400)	F	
II-331SH-A6-401140	W	0.45	3.02	di	0.3 (1400) – 0.2 (2400) – 0.22 (2900)	fsM	$\phi$ -corr sal chg
I-330PZ-A3-400530	AA	0.38	3.0	i	0.18 (1750) – 0.2 (2500)	sM	$\phi$ -corr sal chg
I-330PZ-A4-400600	AB	0.38	3.0	i	0.15 (1850) – 0.3 (2300)	F	$\phi$ -corr sal chg
<b>Figure 4C (Common corner of Blocks 315,330, 329,338)</b>							
I-315MC5-409420	A	0.47	3.16	i	0.25(1450-2020)–0.37(2300)–0.35(2500)	<b>MF</b>	$\phi$ -corr sal chg
I-315EX1-408100	K	0.43	3.0	i	0.25 (1400) – 0.4 (2300)	F	$\phi$ -corr sal chg
I-329EX3-408140	AK	0.43	3.0	i	0.25 (1400) – 0.4 (2200)	F	$\phi$ -corr sal chg
III-330-PZ-D1-410560	AW	0.42	3.2	ic	0.23 (1350) – 0.35 (1800-2400)	bM	
III-330-PZ-9-409830	AU	0.42	3.2	ic	0.2 (1500) – 0.35 (1700-2500)	bM	
III-330-D4ST-411841	BA	0.47	4.1	ic	0.25 (1150) – 0.28 (1150-1400)	bM	
III-330-PZ-B5ST-400951	AY	0.48	3.2	di	0.26 (1550) – 0.20 (1850) – 0.26 (2200)	fsM	
I-329EX2-405660	H	0.38	2.7	c	0.22 (1500-2600)	M	
<b>Figure 4E (Scattered locations S of Block 330)</b>							
I-337PZ3-406580	C	0.49	3.3	c,d	0.25(1600-2750), 0.3(1800)–0.25(3700)	M,fM	$\phi$ -corr sal chg
II-330-PZ-7-401190	AX	0.41	2.53		hydrostatic to 2000 TD		
I-327OXY4-40529	G	0.55	4.16	d	0.25 (1500) – 0.2 (2300)	fM	$\phi$ -unrelated sal chg
I-333MB3-401950	AE	0.43	3.0	c	0.26 (1300-3000)	M	$\phi$ -unrelated sal chg
I-354MB1-406930	I	0.43	3.3	ic	0.15 (2000) – 0.24 (2000-2600)	S2	$\phi$ -corr sal chg
I-337PZ2-406010	B	0.50	3.01	d <sup>3</sup>	0.35(1150-2200), 0.25(2200)–0.15(2900), 0.25(3000)–0.23(3400)	fM <sup>3</sup>	$\phi$ -corr sal chg
I-354MB-A10-409640	AM	0.43	3.0	i	0.24 (1500)–0.36 (2200)	F	$\phi$ unrelated sal chg
I-352AM2-406940	J	0.43	2.95	dic	0.25(1500)–0.23(2100)–0.35(2500-3100)	bM	salinity changes

**Porosity trend:** c=constant, i=increasing, d=decreasing with depth. **Porosity profile:** compartment porosity (depth or depth range[m]). **Genetic type:** M=migrating, F=fixed, s=slow, f=fast, b=buried, S2= Stage 2 compaction, bold indicates that mud weight data confirm disequilibrium compaction pressures calculated from porosity.



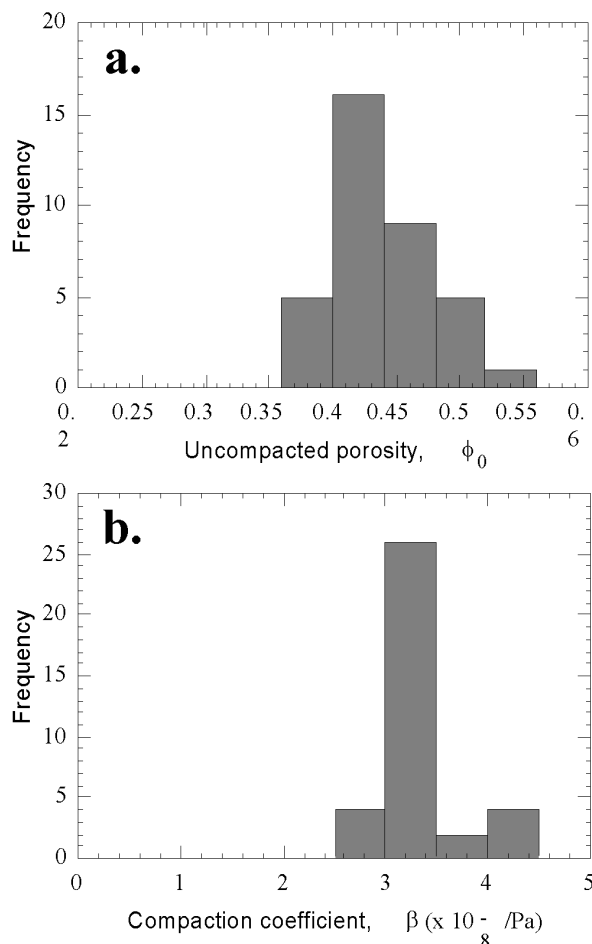


**Figure 5. Compaction parameters determined for the Eugene Island Block 330 study area inverted from the hydrostatic portion of 35 wells.**

We refer to the depth at which porosity departs from hydrostatic in the Figure 4 profiles as the  $\phi$ -DFH depth (DFH = Departs From Hydrostatic), the best fit compaction parameters, and the nature of the porosity profile (increasing, decreasing or constant) are tabulated in Table 1. The  $\phi$ -DFH depths range from 900m to 1950m and the porosities at the  $\phi$ -DFH depths range from 0.3 to 0.15. Figure 6 shows that the  $\phi$ -DFH porosities fall on the hydrostatic compaction curve. The best-fit hydrostatic compaction curve from Figure 2b ( $z_c = 4640$ ,  $\phi_o = 0.43$ ), and the hydrostatic compaction band from a detailed analysis of a single well (Figure 8,  $z_c = 4480$ ,  $\phi = 0.465 \pm 0.015$ ) bracket the  $\phi$ -DFH porosities from Table 1 (solid points in Figure 6). The depth at which porosity departs from the hydrostatic compaction trend is not related to the shale content of the sediments.

Only two profiles show a positive relation between overpressuring and increased shale content (well AW in Figure 4d, and well J in Figure 4e). Five wells show an association of onset of overpressure with drops in sediment shale content (well Y in Figure 4c, wells K and A in Figure 4d, wells AE and I in Figure 4e). Also the profiles cannot be attributed to maximum compaction because sediments in the area clearly can compact to much lower porosities (e.g., 0.15, Figure 6 and Table 1) than are found in the migrating seal compartments.

Figure 7 shows that the  $\phi$ -DFH depths crosscut stratigraphy in the Eugene Island Area. Although Figure 7 shows that  $\phi$ -DFH depths are generally coincident with the top of the 1.27 Ma *H. sellii* horizon just above the gas-charged JD sand, the shallow, 1000m deep  $\phi$ -DFH in Block 314 (Figure 4A) is 500m above the *H. sellii* surface. The porosity-determined top of overpressure thus jumps across two sands and two transgressive shales (Small *Gephyrocapsa* 1 and 2) in this area. Mud weights in 3 wells confirm this interpretation.

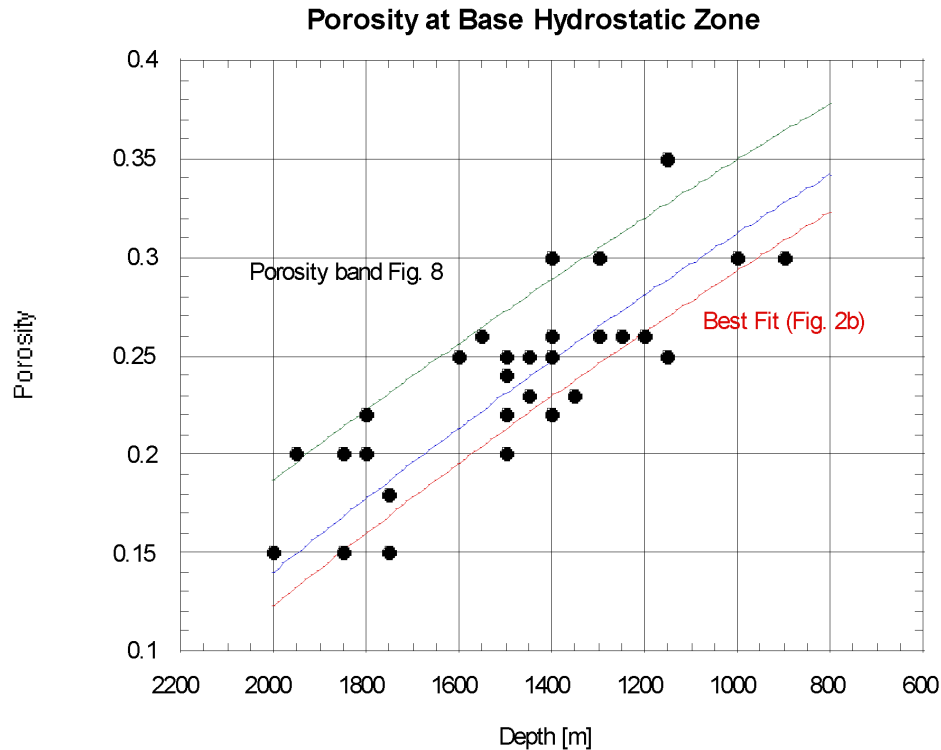


Figure 6. Porosity where the porosity-depth profile departs from hydrostatic,  $\phi$ -DFH, as a function of the depth of the  $\phi$ -DFH. Solid points are from Table 1. Solid lines are hydrostatic compaction curves from Figure 2b (lowest line) and Figure 8a (upper two lines).

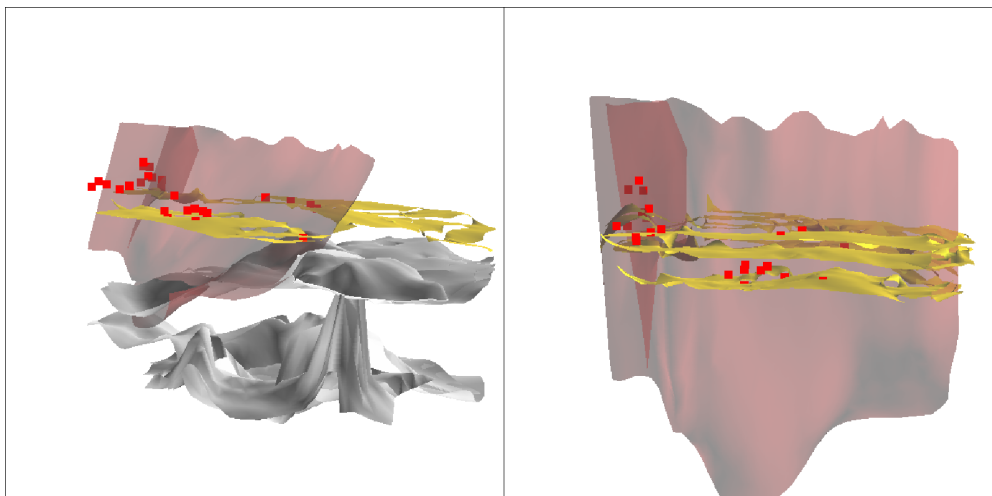
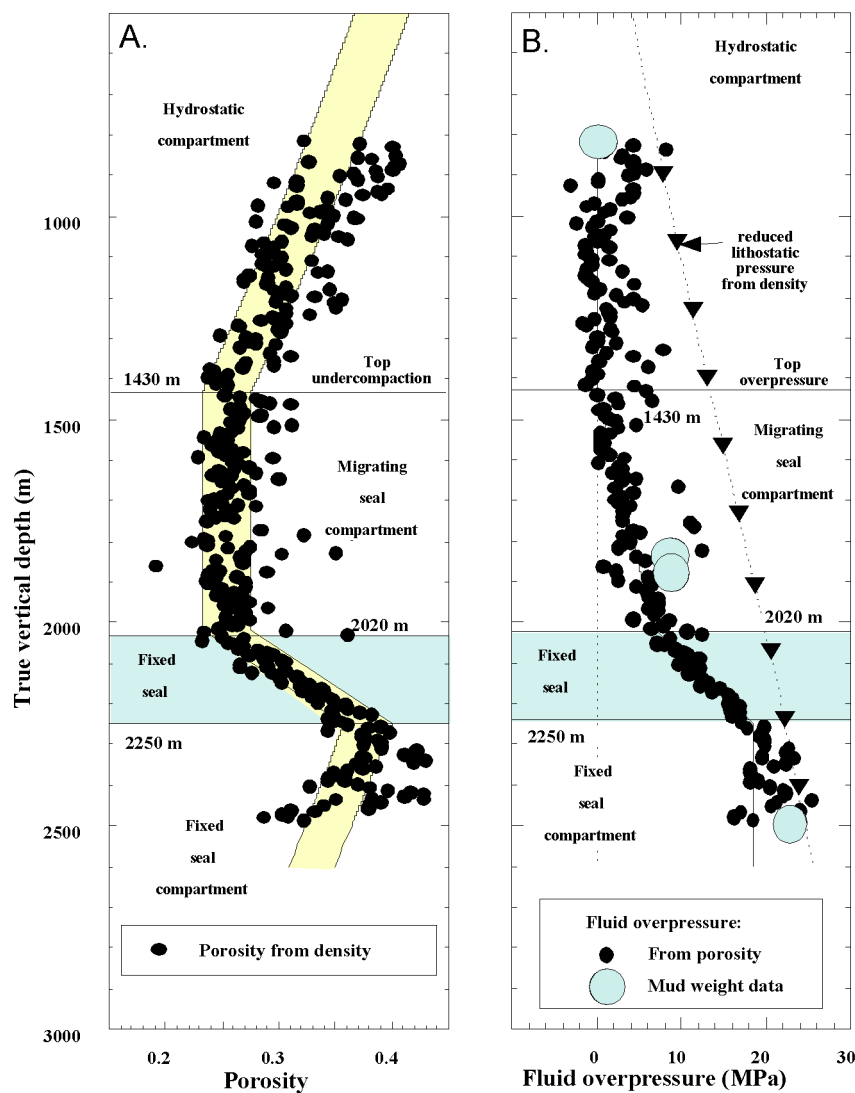


Figure 7. Gocad image of the Pennzoil 3D seismic survey interpreted by Coelho (1997) with extensions into Block 314. The points at which the porosity departs from the hydrostatic porosity-depth profile ( $\phi$ -DFH) are shown (red squares) for the wells in Figure 4 and Table 1. The left hand figure shows the lower salt surface, a salt dome, and an upper salt sill. The single stratigraphic horizon above the salt is the *H. sellii* transgressive shale surface, which immediately overlies the JD sand. The translucent A fault offsets the *H. sellii* horizon, and the C fault can be seen intersecting the A fault in the Block 314 area on the left of the diagram. In the central part of the geologic model, the porosity-determined top of overpressure or  $\phi$ -DFH (square data points) lies along the *H. sellii* surface. However in Block 314, the  $\phi$ -DFH rises stratigraphically and jumps across two overlying sands and two transgressive surfaces to reach  $\sim 1$  km depth (see also Figure 4a). The rise is spatially coherent, as illustrated best in the right frame which shows the faults and sand surfaces (with salt removed) with greater vertical exaggeration.



**Figure 8.** Expanded scale portrayal of porosity profile measure in Well A of Figure 4d. Porosity points were calculated from density log data. Fluid overpressure points and solid curves were calculated using equations developed in text. Theoretical gray band fits the porosity data well. Predicted fluid pressures agree with mud weight data (large gray circles).

Excess fluid pressures are responsible for the excess porosities below the  $\phi$ -DFH. Mud weight data are available for 21 of the 40 wells in Figure 4. The pore pressures calculated from mud weights closely match the pore pressures required to account for the excess porosities, assuming compaction disequilibrium is the cause of the excess porosity. Notice especially where porosity below the  $\phi$ -DFH is constant with depth, the pore pressures measured by mud weight data increase parallel to lithostatic (e.g., wells AG, AF and AN in Figure 4b, wells C and AX in Figure 4e). The constant porosity intervals are thus not examples of Hunt's Stage 2 (arrested) compaction because in this case there would be no reason for the pore pressures to lie so close to the values predicted by disequilibrium compaction. The data confirm that excess porosity is generally a reliable measure of fluid overpressure in the Eugene Island area. Because excess porosity is caused by excess fluid pressure, the  $\phi$ -DFH reflects the depth of onset of fluid overpressuring in the Eugene Island area.

We observe that most often the porosity remains fairly constant below the  $\phi$ -DFH, but sometimes it increases or decreases with depth, and sometimes these changes are quite abrupt (e.g., large changes in

porosity occur over a small depth range). Changes in the salinity-depth profile often reflect changes in the porosity profile. Salinity changes frequently occur at compartment boundaries (Cathles, 2001, this volume), where the porosity profile changes slope or is offset. Sometimes, however, salinity changes are unrelated to porosity boundaries (well G Figure 4e). Faults are the likely cause of some pressure compartmentation (e.g., well AO in Figure 4a, and wells C and B in Figure 4e).

## Interpreting the Porosity Profiles

### Interpretation of the Porosity Pattern in a Single Well

Analytic expressions for lithostatic pressure, fluid pressure, and porosity for the special end-member cases where the fluid pressure is hydrostatic or the porosity is constant over a depth interval are developed in the Appendix. The expressions developed in the Appendix establish a framework for interpreting the porosity-depth profiles in Figure 4. Interpretations can be joined together by matching porosity, fluid pressure, and lithostatic pressure at the boundaries of compartments. The Appendix also derives expressions constraining the depth at which a seal forms, and the depth at which pressure under a seal exceeds 0.8 of lithostatic pressure, the seal begins to leak, and the sediments deform.

Application of expressions in the Appendix to interpreting the porosity profile in a single well is illustrated in Figure 8. First, values are determined for the compaction coefficient,  $\beta$ , and the uncompacted porosity,  $\phi_o$ , which provide the best least squares fit of porosities in the hydrostatically-pressured parts of the well to Equation (6) (Appendix). Taking the grain density equal to 2650 kg/m<sup>3</sup> and the pore fluid density equal to 1100 kg/m<sup>3</sup>, the best fit is provided by  $\beta = 3.16 \cdot 10^{-8}/\text{Pa}$  and  $\phi_o = 0.465 \pm 0.015$ . With these values:  $z_c = 4.48 \pm 0.15$  km and the porosity at the base of the hydrostatic zone at 1430 m is 0.243–0.284 with a mean of 0.263.

The second step in our analysis examines the porosity-depth profile and determines the intervals with constant porosity and the intervals with constant fluid overpressure (e.g., hydrostatically pressured zones where porosity decreases linearly). The porosity profile in Figure 8 is constant with depth from 1430m to 2020m. Porosity then increases sharply with depth to 2250m. Thereafter porosity appears to drop linearly indicating hydrostatic conditions. The compartment boundaries are thus:  $z_{MST} = 1430$  m,  $z_{FST} = 2020$  m,  $z_{FSB} = 2250$  m, and  $\phi_{FSB} = 0.370 \pm 0.015$ . These depths and the porosity at the base of the fixed *H. sellii* seal, together with the values just determined for  $\beta$  and  $\phi_o$ , and equations (14–16), can be used to compute the theoretical porosity-depth profile, and the excess fluid pressure. These are plotted for the range of  $\phi_o$  given above as the shaded band in Figure 8a. The central value of  $\phi_o$  is used to plot the single line in Figure 8b. It is important to note that these profiles are entirely determined by  $\beta$ ,  $\phi_o$ ,  $\phi_{FSB}$ , and the visually determined compartment boundaries  $z_{MST}$ ,  $z_{FST}$ , and  $z_{FSB}$ .

The predicted porosity profile fits the measured data very well. The shaded band in the porosity plot spans most of the solid points where porosity has been determined from the density log. Individual porosity points in the first frame of Figure 8a are converted to pressures using the equations in the Appendix. These pressures are plotted as solid points in Figure 8b. Fluid pressures inferred from mud weight data are plotted as open circles in Figure 8b. The agreement between the predicted overpressures and mud weight data is good, especially considering that drillers usually overweight their mud by 1 to 2 MPa as security against blowouts (e.g., Peska and Zoback, 1995).

The porosity range at the base of the fixed seal ( $\phi_{FSB} = 0.370 \pm 0.015$ ) indicates (via Equation 17, Appendix) that the maximum depth at which the seal could have formed is 0.62–0.84 km, with a most probable depth of 0.73 km. This depth can be visually determined by projecting the porosity at 2250m upward to find the depth where it occurs along the hydrostatic profile in the shallower portions of the porosity profile.

The calculated lithostatic stress at  $z_{FSB}$  is 46.9 MPa and the excess fluid pressure 16.2 MPa. The reduced lithostatic stress is 22.15 MPa. The fluid overpressure is therefore greater than 0.63 times the reduced lithostatic stress (or equivalently, the total fluid pressure is 40.4 MPa, which is greater than 0.8 times the total lithostatic stress). Consequently we predict that the hydrofracture pressure has been

exceeded and the hydrostatic compartment below 2250m has leaked. Sediments in the lower part of the zone labeled fixed seal in Figure 8, therefore, have probably deformed.

Pore fluids draining through the fixed seal decrease pressure in the underling hydrostatic compartment and uniformly decrease the porosity in this compartment as effective stress increased. The fixed seal could therefore have formed at depths shallower than the 0.62–0.84 km calculated above. If the fixed seal forms at 530 m, according to our calculations (Equation 19, Appendix) it would have started deforming at 1430m (the present depth of the constant porosity compartment). Thus, the constant porosity compartment could be produced by leakage from the hydrostatically pressured compartment labeled “fixed seal compartment” in Figure 8a. The fixed seal and its compartment must have formed before the constant porosity compartment developed because the fixed seal formed at a depth that is less than half the depth of the present top of the constant porosity interval (1430 m).

The above discussion shows that the methods we have developed allow a good deal of information to be extracted from a porosity profile. It is interesting that the seals must have formed at relatively shallow depths (probably about 530 m below sea floor). Sealing occurs early, and the fixed seal is then buried. The fixed seal lies near the 1.27 Ma *H. sellii* horizon (Figure 1). AS the sedimentation rate is about 2 km/Ma, the fixed seal has formed at about 1 Ma and subsequently has been buried to its present depth. The fixed seal starts to deform and leak when it reaches a depth of 1400 m, about 0.7 Ma. A constant porosity compartment then grew on top of the fixed seal compartment as it leaked.

### Physical Interpretations of the End Member Porosity Profiles

There are at least several possible physical interpretations of how hydrostatic and fixed porosity compartments might develop. So far we have defined these compartments only mathematically as zones of constant porosity or intervals of hydrostatic (but elevated) fluid pressure. Consider now some possible physical explanations of the two types of compartments.

The origin of what we call a fixed seal pressure compartment is the easiest to understand. A fixed seal pressure compartment results when the strata above the compartment become impermeable but the strata within the compartment are still permeable. A fixed seal could form at the surface by the deposition of an impermeable sediment layer. Alternatively a fixed seal could form when a sediment layer becomes impermeable after it is buried to some depth. Permeability is a strong function of porosity, so this could occur as the result of normal compaction, perhaps aided by compaction-related induration as suggested by Ortoleva, (1994, and references therein). It could also occur with the introduction of a non-aqueous fluid phase and the formation of capillary barriers or by clay dewatering (Gordon and Flemings, 1998). The distinguishing characteristic of a fixed seal pressure compartment is that, within this compartment, fluid pressure increases with depth along a hydrostatic gradient. Excess fluid pressure within the compartment is constant. Well AB in Figure 4c provides an example of this. Shale porosity decreases in a hydrostatic fashion, parallel to the hydrostatic compaction profile seen higher in the hole. Importantly, because hydrostatic fluids must communicate freely, if the fixed seal is ruptured, the fixed seal pressure compartment will expel fluid until the entire compartment is depressured.

The physical requirements for the formation of a constant porosity pressure compartment (*i.e.*, migrating seal compartment) can also be clearly stated and are also quite restrictive. For porosity to remain constant where compaction disequilibrium applies, fluid pressure must increase with depth parallel to lithostatic pressure so that effective stress remains constant. There must therefore be a strong vertical gradient in excess fluid pressure in the interior of a migrating seal compartment, yet it drives no fluid movement. A migrating seal pressure compartment thus cannot be permeable. Unlike a fixed seal compartment, fluids within this compartment are not free to circulate, and cannot vent rapidly if the migrating seal is ruptured. The interior of a migrating seal compartment may be pressure-compartmented by a honeycomb of seals, or the sediments within it may simply be intrinsically impermeable. The excess pore pressures in the compartment could in principle be generated internally or established by external factors.

Pore pressures are locally generated in the disequilibrium compaction model presented by Gordon and Flemings (1998). Their constant porosity compartment is overpressured as a result of decreasing sediment permeability during burial compaction. The permeability must decrease with depth in a very specific way for compaction disequilibrium to create an interval of constant porosity in the subsurface.



If sedimentation rates decrease, fluid pressures will decay. If constant porosity in the migrating seal compartment is to be maintained, the pressure decay must also be such that fluid pressures still parallel the lithostatic gradient, and effective stress remains constant.

A constant porosity profile can also be produced by a seal, which responds to sedimentation by moving or migrating in the section. If the migrating seal moves upward at the sediment accumulation rate, porosities equal to that of the seal would be trapped, and a constant porosity interval would result if the migrating seal compartment were impermeable. The impermeability of the migrating seal compartment would assure that fluid pressures within the compartment increase with each increment of added sediment load and therefore that the fluid pressure profile would continue to parallel the lithostatic gradient. The key conclusion inherent in this seal formation mechanism is that sediments become impermeable at a constant depth.

Hydrate seals in the Mediterranean provide an example of how external factors could produce a migrating seal. Porosity in that area decreases along a hydrostatic compaction profile to a depth of about 150 m. Porosity is constant below this depth in all but one drill hole (Shipboard Scientific Party, 1996). In that one drill hole, porosity increases with depth below what appears to be a fixed seal (Revil *et al.*, 1998), but the profile may be corrupted because of coincident changes in hole-diameter (A. Brown, personal communication, 1998). Excepting that hole (which unfortunately was the only one we chose to interpret in Revil *et al.*, 1998), the porosity profiles are exactly of the form expected for a migrating seal.

It appears in this area that a hydrate layer forms the top of the migrating seal compartment and traps gas below. Hydrates can be the most impermeable seal type, better even than evaporites (Hunt, 1996, p. 278). Because the hydrates form at an isotherm, the hydrate seal maintains a constant depth below the sediment-water interface as sedimentation proceeds. The result is a constant porosity interval spanning the depth interval across which the hydrate seal has migrated. Gas capillary effects could maintain sealing below the hydrate layer and prevent compaction and the equilibration of overpressures in the migrating seal compartment. Gas could migrate upward as the hydrate seal breaks down thermally, and the impermeable zone could grow with time exactly as described above, producing a migrating seal porosity profile. The Mediterranean example suggests that “externally controlled” migrating seals are possible.

The migrating seal porosity profiles at Eugene Island form at depths too great (1000m, 1400–2000 m) for them to be hydrate seals. Hydrates break down at temperatures of at most ~23°C (Sloan, 1998). However, the migrating seal compaction profiles in the Eugene Island area could form when hydrocarbons are introduced and capillary seals formed at the interfaces of fine and coarse-grained sediments (*e.g.*, Shosa and Cathles, 2001, this issue).

### Interpretation of the Eugene Island Area

The fixed seal portion of the well analyzed above (Fig. 8) is typical of fixed seal profiles in the Eugene Island Block 330 study area. Examination of Figure 4 and Table 1 shows that the porosities at the base of fixed seals are often >0.35, despite lying at depths of ~2 km or more. The fixed seal profiles in about 6 wells (marked F in genetic column of Table 1) suggest sealing occurred early (~1.27 Ma) and at shallow depths (<~530 m).

The porosity-depth profiles in Figure 4 are clearly not all of either of the fixed or migrating seal end-member type, although most are closer to one or the other of the two. All the porosity-depth profiles can be understood and interpreted in terms of the two end-member curves, however.

Injection of hydrocarbons will produce a honeycomb of capillary compartments in the interlayered fine-coarse sediment lozenges within the migrating seal compartment. Variable rates of hydrocarbon injection (and seal migration) can account for the variations in migrating seal profiles observed in Figure 4. If hydrocarbons are introduced at a rate such that the top of the sealed compartment moves upward at the same rate as sediment deposition, an end-member migrating seal compartment (M) having constant porosity will result. If hydrocarbon is introduced at a slower rate, the top of the migrating seal compartment will be slowly buried, and the compartment porosity will increase with depth because higher porosities are trapped earlier when the seal was shallower and lower porosities were trapped later when the seal was deeper. In Table 1 we refer to this as a slow migrating (sM) seal. Conversely, if hydrocarbon sealant is introduced at a faster rate than the rate of sedimentation, the top of the fast migrating



(or fM) seal compartment will rise to shallower depths with time, and the compartment porosity will decrease with depth because lower porosity sediments were preserved when the seal was deeper. Finally, if the supply of hydrocarbon sealant is cut off, the compartment will cease growing, and it will be buried by subsequent sedimentation (bM for buried migrating seal). Compaction will continue in a hydrostatic zone above the migrating seal compartment, but the porosity within the compartment will not change. With time, the compartment porosities will become increasingly displaced relative to the overlying hydrostatically compacted sediments. The offset to higher porosities at the top of the compartment will appear similar to a fixed seal profile, but below the transition to higher porosities the porosity profile will be constant, rather than decreasing with depth as it does in a fixed seal compartment.

If sealing is related to the introduction of hydrocarbons, porosity profiles convey important information about how and when hydrocarbons migrated. A buried migrating seal profile (bM) indicates an area where hydrocarbon migration was more active in the past than at present. Fast migrating (fM) profiles flag areas where the introduction of hydrocarbons is occurring at unusually rapid rates. Fixed seal (F) porosity profiles identify areas where fluids can move laterally (through the permeable fixed seal compartments) to topographic highs in the top of overpressure. Fluids will leak at these topographic highs, because as overpressures build they will be the locations where the fluid pressures will first exceed lithostatic. Fixed seal profiles are of interest also because they suggest that sands within the fixed seal compartment will have unusually high porosity. If filled with hydrocarbons, these sands will be especially attractive exploration targets, *i.e.*, they will contain more oil per unit volume and have much higher permeability because sand permeability is a power law function of porosity.

Examining the Eugene Island study area in the above context, the very shallow migrating seal compartments and the fast migrating seals in its northwestern parts (Blocks 314, 331 and western 330) suggests hydrocarbon leakage may be most active there. The fixed seals and the buried migrating seals in the northern and western parts of Block 330 and to the south (Fig. 4e) suggest hydrocarbon migration may have decreased and/or become more focused in those areas.

## Conclusions

Our analysis of the Eugene Island Block 330 area shows that the departures of shale porosity from the hydrostatic compaction trend are coherent and provide significant new information on the possible nature of seals. The departure of shale porosity from the hydrostatic compaction trend is caused in this area by the development of pore pressures in excess of hydrostatic, and thus the departure of porosity from its hydrostatic profile provides a useful definition of the top of overpressure. We provide mathematical tools to interpret these departures (Appendix). Without theoretical guide curves showing the expected hydrostatic compaction, however, interpretation is extremely difficult. The guide curves, although seemingly trivial, are thus important. The porosity-determined top of overpressure surface is coincident over much of the study area with the *H. sellii* transgressive shale. However there is more information in the porosity profiles than just determination of the depths at which overpressuring begins. In the Eugene Island vicinity there are areas where the porosity is constant with depth, increases or decreases slowly with depth, and increases sharply with depth and then decreases. In a relatively complexly faulted area of Block 314, the porosity-determined top of overpressure cuts across two sands and two transgressive surfaces in a cylindrical, vent-like protuberance. We have interpreted these profiles in terms of fixed and several types of dynamic (migrating) seals. We acknowledge that there may be other explanations for the different porosity profiles identified.

We relate seal dynamics to the injection of hydrocarbons and the development of capillary barriers at the boundaries of fine and coarse-grained sediments. We identify parts of the study area where hydrocarbon injection appears to be accelerating, and areas where it appears to be declining or have recently terminated. Beneath what we term fixed seals, the porosity of sands just below the top of the overpressured compartment is much greater than in similar positions beneath a migrating seal. The sands below fixed seals are more permeable because of their greater porosity, store more hydrocarbon per unit volume, and are much more attractive exploration prospects. The spatial coherency of porosity profile type is an important observation because it implies that the location of high permeability sand might be pre-



dicted. Also, if porosity profiles are interpreted to reflect hydrocarbon leakage, our analytical analysis indicates that they also contain important information on the timing of the leakage.

## Acknowledgments

The authors thank Elf Aquitaine for supporting Andre Revil's post-doctoral study at Cornell University during which time the work reported here was carried out. Support is also gratefully acknowledged from the Gas Research Institute (Grant 35093-260-2689) and the member companies of the Global Basins Research Network. We thank Mike Wizevich for preparing the GoCAD images in Figure 7.

## References

- Alexander, L. L., 1995, Geologic evolution and stratigraphic controls on the fluid flow of the Eugene Island Block 330 Minibasin, offshore Louisiana: Ph.D. thesis, Ithaca, Cornell University, 206 p.
- Alexander, L. L., and P. B. Flemings, 1995, Geologic evolution of a Pliocene-Pleistocene salt withdrawal minibasin: Eugene Island Block 330, offshore Louisiana: AAPG Bull., v. 79, p. 1737–1756.
- Alexander, L. L., and J. W. Handschy, 1998, Fluid flow in a faulted reservoir system: fault trap analysis for the Block 330 field in Eugene Island, South Addition, offshore Louisiana: AAPG Bull., v. 82, p. 387–411.
- Bangs, N. L., G. K. Westbrook, J. W. Ladd, and P. Bulh, 1990, Seismic velocities from the Barbados Ridge complex: indicators of high pore pressures in an accretionary complex: Jour. Geophysical Research, v. 95, p. 8767–8782.
- Bour, O., I. Lerche, and D. Grauls, 1995, Quantitative models of very high fluid pressure: the possible role of lateral stress: Terra Nova, v. 7, p. 68–79.
- Bray, C. J., and D. E., Karig, 1985, Porosity of sediments in accretionary prisms and some implications for dewatering processes: Jour. Geophysical Research, v. 90, p. 768–778.
- Cathles, L. M., 2001, Capillary seals as a cause of pressure compartmentation in sedimentary basins: GCSSEPM Foundation 21st Bob F. Perkins Research Conference, this issue.
- Coelho, D., 1997, Three dimensional analysis of the temperature field in Block 330, South Eugene Island, Gulf of Mexico: Ph.D. thesis, Cornell University, 292 p.
- Fertl, W. H., 1976, Abnormal formation pressure, implications for exploration, drilling, and production of oil and gas resources: Elsevier, Amsterdam, 382 p.
- Fowler, W. A., 1970, Pressures, hydrocarbon accumulation and salinities—Chocolate Bayou field, Brazoria County, Texas: Jour. Petroleum Technology, v. 22, p. 411–423.
- Gordon, D. S., and P. B. Flemings, 1998, Two-dimensional modeling of groundwater flow in an evolving deltaic environment: SEPM, v. 62, p. 301–312.
- Hart, B. S., P. B. Flemings, and A. Deshpande, 1995, Porosity and pressure: role of compaction disequilibrium in the development of geopressure in a Gulf Coast Pleistocene basin: Geology, v. 23, p. 45–48.
- Holland, D. S., J. B. Leedy, and D. R. Lammelin, 1990, Eugene Island Block 330 field—USA, offshore Louisiana, in Beaumont, E.A., and Foster, N.H., eds., Structural Traps; III, Tectonic fold and fault traps: Treatise of Petroleum Geology Atlas of Oil and Gas Fields, AAPG, p. 103–143.
- Hunt, J. M., 1996, Petroleum Geochemistry and Geology: W. H. Freeman, New York, 743 p.
- Hunt, J. M., J. K. Whelan, L. B. Eglinton, and L. M. Cathles III, 1998, Relation of shale porosities, gas generation, and compaction to deep overpressures, in the U.S. Gulf Coast, in Law, B. E., G. F. Ulmishek, and V. I. Slavin, eds, Abnormal pressures in hydrocarbon environments: AAPG Memoir 70, p. 87–104.
- Losh, S., L. Eglinton, M. Schoell, and J. Wood, 1999, Vertical and lateral fluid flow related to a large growth fault, South Eugene Island Block 330 Field, offshore Louisiana: AAPG Bull., v. 83, p. 244–276.
- Luo, X. R., and G. Vasseur, 1992, Contributions of compaction and aquathermal pressuring to geopressure and the influence of environmental conditions: AAPG Bull., v. 76, p. 1150–1159.
- Luo, X. R., and G. Vasseur, 1993, Contributions of compaction and aquathermal pressuring to geopressure and the influence of environmental conditions: reply: AAPG Bull., v. 77, p. 2011–2014.
- Magara, K., 1978, Compaction and Fluid Migration, Practical Petroleum Geology, Elsevier, New York, 319 p.
- Ortoleva, P. J., 1994, Basin Compartmentation: definitions and mechanisms, in P. J. Ortoleva, ed., Basin Compartments and Seals, AAPG Memoir 61, Tulsa, 3–26, p. 39–51.
- Peska, P., and M. D. Zoback, 1995, Compressive and tensile failure of inclined well bores and determination of *in situ* stress and rock strength, J. Geophys. Res., 100, p. 12791–12811.
- Revil, A., L. M. Cathles, J. D. Shosa, P. A. Pezard, and F. D., de Larouziers, 1998, Capillary sealing in sedimentary basins: a clear field example, Geophysical Research Letters, v. 25 no. 3, p. 389–392.



- Shi, Y., and C., Wang, 1988, Generation of high pore-pressures in accretionary prism: inferences from the Barbados subduction complex, *Jour. Geophysical Research*, v. 93, p. 8893–8910.
- Shipboard Scientific Party, 1996, *in* R. N. Riegel, ed.: *Proceedings, Ocean drilling Program Initial Report*, v. 161, College Station, Texas.
- Shosa, J. D., and L. M. Cathles, 2001, Experimental investigation of capillary blockage of two phase flow in layered porous media: GCSSEPM Foundation 21st Bob F. Perkins Research Conference, this issue.
- Sloan, E. D., 1998, *Clathrate hydrates of natural gases*: Marcel Dekker, Inc., New York, 705 p.
- Storer, A., 1959, *Constiparmento dei sedimenti argillosi nel Bacino Padano: Giacimenti Gassiferi dell' Europa Occidentale*, *Acad. Nazionale dei Lincei*, Rome, p. 519–544.
- Stump, B. B., P. B. Flemings, T. Finkbeiner, and M.D. Zoback, 1998, Pressure differences between overpressured sands and bounding shales at the Eugene Island 330 field (offshore Louisiana, USA) with implications for fluid flow induced by sediment loading, *in* A. Mitchell, and D. Grauls, eds., *Overpressures in Petroleum Exploration, Workshop Proceedings: Memoir 22*, Elf EP-Editions, Pau, France, p. 83–92.
- Zoback, M. D., and P. Peska, 1995, *In situ*-stress and rock strength in the GBRN/DOE Pathfinder well, South Eugene Island, Gulf of Mexico, *Jour. of Petroleum Technology*, v. 5, p. 582–585.

## Appendix

We assume that changes in porosity,  $d\phi$ , are explicitly related to changes in effective stress,  $d\sigma_{eff}$  :

$$d\phi = -\phi_o\beta d\sigma_{eff} \quad (1)$$

where  $\phi_o$  is the uncompacted porosity and  $\beta$  is the long term compressibility. The effective stress equals the lithostatic stress,  $P$ , minus the pore pressure,  $p$ :

$$\sigma_{eff} = P - p \quad (2).$$

Lithostatic stress is related to the density of the mineral grains,  $\rho_g$ , the density of the pore fluid,  $\rho_f$ , and sediment porosity,  $\phi$  :

$$dP(z) = (\rho_g(1 - \phi) + \rho_f\phi)gdz \quad (3)$$

### Hydrostatic Porosity Profiles

Under hydrostatic conditions (indicated by the subscript  $H$ ):

$$\begin{aligned} dP_H(z) &= (\rho_g(1 - \phi_H) + \rho_f\phi_H)gdz, \\ dp_H(z) &= \rho_fgdz \end{aligned} \quad (4)$$

$$d\sigma_{eff} = dP - dp$$

$$d\sigma_{eff} = (1 - \phi)(\rho_g - \rho_f)gdz.$$

Thus, by (1):

$$d\phi = -\phi_o\beta(1 - \phi)(\rho_g - \rho_f)gdz \quad (5)$$

which can be integrated from the surface to depth  $z$  to give:

$$\phi_H = 1 - (1 - \phi_o)\exp(z/z_c), \text{ in Stage 1 Compaction} \quad (6)$$

$$\phi_H = \phi_L = \text{constant}, \text{ in Stage 2 Compaction}$$

In (6)  $z_c \equiv 1/\phi_o\beta g(\rho_g - \rho_f)$ , and  $\phi_L$  is the shale porosity at the limit of normal compaction (top of Stage 2). The lithostatic pressure in a hydrostatically pressured section,  $P_H$  can be obtained by substituting Eq. (6) into (3), and integrating from 0 to  $z$ , which yields:

$$P_H(z) = \rho_fgz + g(\rho_g - \rho_f)(1 - \phi_o)z_c \left[ \exp\left(\frac{z}{z_c}\right) - 1 \right] \quad (7)$$

Of course,

$$P_H = \rho gz \quad (8)$$

where  $\rho = \rho_g(1 - \phi) + \rho_f\phi$  is the total sediment density. Defining the departure from hydrostatic pore pressure, lithostatic pressure, and porosity by  $\delta p$ ,  $\delta P$ , and  $\delta\phi$ , we can write without loss of generality:

$$p = p_H + \delta p$$



$$P = P_H + \delta P \quad (9)$$

$$\phi = \phi_H + \delta\phi$$

Substituting Eqs. (6)–(8) yields:

$$p = \rho_f g z + \delta p$$

$$P = \rho_f g z + (\rho_g - \rho_f) g z_c (1 - \phi_o) \left[ \exp\left(\frac{z}{z_c}\right) - 1 \right] + \delta P \quad (10)$$

$$\phi = 1 - (1 - \phi_o) \exp\left(\frac{z}{z_c}\right) + \delta\phi$$

By (1) the porosity change  $\delta\phi$  is related to the effective stress change,  $\delta P - \delta p$ , by:

$$\delta\phi = -\phi_o \beta (\delta P - \delta p) \quad (11)$$

and substituting (9) into (3) and using (4a) gives:

$$\delta P = -\int_0^z (\rho_g - \rho_f) g \delta\phi dz' \quad (12)$$

Combining (11) and (12), and using the definition of  $z_c$  in (6) yields:

$$\delta p(z) = \frac{1}{\phi_o \beta} \left( \delta\phi(z) - \frac{1}{z_c} \int_0^z \delta\phi(z') dz' \right), \text{ in Stage 1 Compaction} \quad (13)$$

$$\delta p(z) = \text{unconstrained, in Stage 2 Compaction.}$$

Equations (12) to (13) are exact in the sense that they do not result from any approximation other than the disequilibrium compaction assumption that porosity and effective stress are related as shown in (1). These equations give excess lithostatic and pore pressure as functions of excess porosity. Together with the hydrostatic equations (6) and (7) they provide an important reference for interpretation of departures from hydrostatic compaction and the pattern of “anomalous” porosity profiles in the South Eugene Island Block 330 area.

### The Special Case Where Porosity is Constant in a Pressure Compartment

Consider the case where porosity is constant over an interval of depth:

$$\phi = \phi_{MST} = \phi_H + \delta\phi \quad (14a)$$

Here the subscript *MST* stands for Migrating Seal Top. For reasons discussed in the text we call this depth interval a migrating seal compartment. Substituting  $\phi_H$  from (6) into (14a), and using (9) and (6) to convert  $\phi_{MST}$  to  $\delta\phi_{MST}$  gives:

$$\delta\phi_m = \delta\phi_{MST} + (1 - \phi_o) \left\{ \exp\left(\frac{z}{z_c}\right) - \exp\left(\frac{z_{MST}}{z_c}\right) \right\} \quad (14b)$$

Here the subscript *m* indicates the equation applies within a migrating seal compartment where porosity is constant and equal to  $\phi_{MST}$ , and the excess porosity at the top of the migrating seal compart-



ment is  $\delta\phi_{MST}$ . Substituting (14b) into equations (12) and (13) and integrating gives  $\delta P_m$  and  $\delta p_m$ , the excess lithostatic pressure and the excess fluid pressure as a function of depth:

$$\delta P_m(z) = \delta P_{MST} + (\rho_g - \rho_f)g(1 - \phi_{MS}) \left[ (z - z_{MST}) \exp\left(\frac{z - z_{MST}}{z_c}\right) - z_c \left( \exp\left(\frac{z}{z_c}\right) - \exp\left(\frac{z_{MST}}{z_c}\right) \right) \right] \quad (14c)$$

$$- (\rho_g - \rho_f)g(z - z_{MST})\delta\phi_{MST}$$

$$\delta p_m(z) = \delta p_{MST} + (\rho_g - \rho_f)g \left[ (1 - \phi_{MS})(z - z_{MST}) + (1 - \phi_o)z_c \exp\left(\frac{z - z_{MST}}{z_c}\right) \right] \quad (14d)$$

$$- (\rho_g - \rho_f)g(z - z_{MST})\delta\phi_{MST}$$

### The Special Case Where Excess Hydrostatic Pressure is Constant in a Pressure Compartment

The other end-member case is a pressure compartment in which the fluid overpressure is constant over a depth interval:

$$\delta P_f(z) = \delta p_{FSB} = \text{constant, or } d\delta p_f(z) = 0 \quad (15a)$$

We call this depth interval a fixed seal pressure compartment, and indicate the equations apply inside this compartment with a subscript  $f$ .  $\delta p_{FSB}$  is the excess fluid pressure at the base of the fixed seal. Differentiating (11), substituting (15a) and (12), separating variables and integrating yields:

$$\delta\phi_f(z) = \delta\phi_{FSB} \exp\left(\frac{z - z_{FSB}}{z_c}\right) \quad (15b)$$

where  $\delta\phi_{FSB}$  is the excess porosity at the base of the fixed seal and  $z_{FSB}$  is the depth of the base of the fixed seal. Excess lithostatic pressure is obtained by substituting (15b) into (12) and integrating. The result is:

$$\delta P_f(z) = \delta P_{FSB} + (\rho_g - \rho_f)gz_c \delta\phi_{FSB} \left[ 1 - \exp\left(\frac{z - z_{FSB}}{z_c}\right) \right] \quad (15c)$$

$\delta P_{FSB}$  is the excess lithostatic pressure at the base of the fixed seal.

The porosity at the base of the fixed seal is a free variable whose value depends on the depth at which the seal formed and how much the seal has leaked. The porosity at the base of the fixed seal is  $\phi_{FSB}$  and the excess porosity can be determined using (6) and (9). The average porosity in the seal itself is then:

$$\bar{\delta\phi}_{FS} \approx \frac{\delta\phi_{FSB} + \delta\phi_{FST}}{2} \quad (16a)$$

where  $\delta\phi_{FST}$  is the excess porosity at the top of the fixed seal. By (12) excess lithostatic pressure at the base of the fixed seal is related to that at the top:

$$\delta P_{FSB} = \delta P_{FST} + (\rho_g - \rho_f)g\bar{\delta\phi}_{FS}(z_{FST} - z_{FSB}) \quad (16b)$$

where  $z_{FST}$  and  $z_{FSB}$  are the depths to the top and bottom of the fixed seal. Finally excess fluid pressure can be obtained from the excess porosity and excess lithostatic pressure (16a) at the base of the fixed seal using (11):



$$\delta p(z) = \delta P_{FSB} + \frac{\delta \phi_{FSB}}{\phi_o \beta} \quad (16c)$$

### The Maximum Depth of Seal Formation

Porosities at the base of a fixed seal and at the top of a migrating seal constrain the depths and therefore times when the seals formed. The maximum depth at which a fixed seal could have formed and the depth at which a migrating seal did form are provided by substituting  $\phi_{FSB}$  or  $\phi_m$  for  $\phi_H$  in (6):

$$z_{maxFS}^f = z_c \ln\left(\frac{1 - \phi_{FSB}}{1 - \phi_o}\right), z_m^f = z_c \ln\left(\frac{1 - \phi_m}{1 - \phi_o}\right) \quad (17)$$

Here  $z_{maxFS}^f$  is the maximum depth of formation of a fixed seal as a function of  $\phi_{FSB}$ , and  $z_m^f$  is the depth of formation of a migrating seal as a function of  $\phi_m$ , the porosity in the migrating seal compartment. Depth is constrained because if the depth of seal formation were too great, sediments below the seal would have compacted to porosities lower than those observed. The fixed seal could have formed at shallower depths because it could have leaked and reduced fluid pressure in the fixed seal compartment. Thus, in this case, the depth is an upper bound, not an actual measure of the depth of formation. Leakage of a migrating seal cannot relieve fluid pressures in its underlying compartment as easily because it is impermeable (micro-compartmented). The depth of formation of the migrating seal is thus more likely to be indicated directly by its porosity.

### The Depth of Sediment Deformation

Fluid pressures can approach lithostatic in the subsurface. Pressures 93 % of lithostatic have been measured at Eugene Island (Hart *et al.*, 1995) and fluid pressures 98% of lithostatic have been inferred (Losh *et al.*, 1999). However, for fluid pressures to closely approach lithostatic the stress tensor must be isotropic- horizontal stress must approach vertical stress more closely than is typical under normal subsurface conditions where the horizontal stress is ~0.8 times the vertical. Thus when fluid pressures exceed about 0.8 times the vertical stress, the sediments must deform in a way that causes the lithostatic stress to become more isotropic. This deformation will begin to occur when:

$$p \geq 0.8P$$

$$\delta p \geq 0.63(P - p_H) \quad (18)$$

where the second equation is an approximation of the first obtained by assuming that  $P/p_H \sim 2.2$ . Since the excess pressure under a fixed seal that has not leaked equals the reduced lithostatic load added since seal formation, a fixed seal will begin to deform when:

$$(P - p)_{zdef} - (P - p)_{zfm} > 0.63(P - p)_{zdef}, \text{ or}$$

$$(P - p)_{zdef} > 2.7(P - p)_{zfm} \quad (19)$$

Here the subscript *zdef* indicates the expression in parentheses should be evaluated at the depth where the seal begins to deform, and the subscript *zfm* indicates the expression should be evaluated at the depth of seal formation.

Equation (19) shows that deformation of a fixed seal will occur when the seal is buried to roughly 2.7 times the depth of sealing. If the seal forms at the surface it will deform from the beginning. If it forms at 500 m depth, it will deform at about 1350 m. If the overlying sediments are hydrostatically pressured,  $p$  and  $P$  in (19) can be given a subscript  $H$ , and equations (7) and (8) can be used to calculate the depth of deformation more accurately. Deformation will begin in a migrating seal when (18) is met. We assume that the tensile strength of the Eugene Island sediments is very low and so all seals must and will leak if the fluid pressure exceeds lithostatic. The seal may begin to leak when it starts to deform.



---

## Modeling Methodology

This completes a modular, end-member description of pressure compartmentation in basins. With the translation equations (9), the equations for the hydrostatic zone (6-8), migrating seal compartment (14a-d), fixed seal (16a-c), and fixed seal compartment (15a-c), porosity, lithostatic pressure, and fluid pressure can be described in stacked hydrostatic, migrating and fixed seal compartments. There can be any number of fixed or migrating seal compartments and the stacking can be in any order. The description is therefore quite flexible. The only assumption is that porosity is related to effective stress as indicated by (1). For specified values of the uncompacted porosity,  $\phi_0$ , and compressibility,  $\beta$ , the compaction profile is entirely specified by the depths of the compartment boundaries and the porosity at the base of fixed seals.

